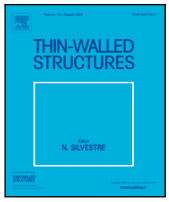
Thin-Walled Structures 182 (2023) 110150



Contents lists available at ScienceDirect

Thin-Walled Structures

journal homepage: www.elsevier.com/locate/tws



Full length article

Elastic local buckling formulae for thin-walled I-sections subjected to shear and direct stresses



Luke Lapira *, Leroy Gardner, M. Ahmer Wadee

Department of Civil and Environmental Engineering, Imperial College London, South Kensington Campus, London SW7 2AZ, UK

ARTICLE INFO

Keywords:
Buckling
Shear
Plate girder
Eurocode
Local instability
Plate buckling
Structures

ABSTRACT

Formulae for calculating the elastic local buckling stresses of doubly-symmetric thin-walled I-section girders subjected to combined shear and direct stresses, accounting for the interaction between the plate elements are presented. The interaction between the plate elements (i.e. the flanges and web) is bounded by a theoretical lower-bound, where there is no interaction and the critical plate is considered to be simply-supported, and a theoretical upper-bound where interaction is strongest and the critical plate is considered to have rotationally fixed edges. The interaction is accounted for by introducing an interaction coefficient ζ that quantifies the relative level of fixity between the aforementioned lower and upper bounds. Expressions to calculate ζ are calibrated using results from finite element analyses generated in Abaqus. Doubly-symmetric I-sections of varying geometric proportions loaded in shear, major axis bending, compression and a full range of combinations thereof are considered. Using the developed formulae, the elastic local buckling stresses of the studied cross-sections are accurately predicted, typically within 5% of the values obtained from FE models; this is a significant improvement over the results determined in the traditional manner in which plate element interaction effects are ignored, where the full cross-section buckling stress is shown to be underestimated by as much as 40%.

1. Introduction

Thin-walled I-sections are used in a very wide range of applications and are designed to withstand axial force, bending moment and shear forces applied during the life-span of a structure. The approach to the local stability design of such sections presently adopted in structural design codes, such as EN 1993-1-5 [1], considers the flanges and web as individual plate elements with simply-supported boundary conditions buckling in isolation. However, it has been shown that for any load case considered, the buckling stress of the cross-section when considered in its entirety is generally larger than that of the individual plates with simply-supported boundary conditions [2–4]. This higher buckling stress is attributed to the fact that the individual plate elements that form the cross-section do not buckle in isolation, but interact with each other, with the more slender plates receiving additional restraint from the less slender plates [4]. Stowell and Lundquist [5] used the energy method to analyse the elastic buckling stress of I-, Z-, C- and rectangular hollow sections under axial compression. The same authors later presented research demonstrating how the buckling stress of rectangular plates increases with increasing rotational edge fixity [6,7].

Gardner et al. [4] developed a methodology to determine the full cross-section elastic local buckling stress for a wide range of structural cross-sections subjected to compression, bending and their combined actions. The methodology was based on the premise that the buckling stress of the entire cross-section lies within the boundaries established by the buckling stress of isolated critical plates with simply-supported and rotationally fixed boundary conditions along the adjoining plate edges. The authors [4] used the finite-strip method (FSM) to calibrate predictive formulae for an interaction coefficient ζ that defines where the full cross-section elastic local buckling stress lies between the aforementioned upper and lower bounds. Excellent agreement between predicted buckling stresses using the developed model and a substantial range of numerical results was demonstrated for a variety of structural cross-sections from American and European databases.

Similar efforts to determine the elastic buckling stress of full cross-sections subjected to shear have also been reported. Lee et al. [8] carried out a parametric finite element (FE) study on approximately 300 plate girder models to investigate the effect of geometric parameters on the buckling stress for I-sections subjected to shear stress. Based on the numerical results, a predictive model was then developed, in which account was taken of the effect of the flange on the critical web buckling stress, but the susceptibility of the flange to shear buckling was not considered. Pham and Hancock [2] used a spline FSM to study a variety of stress distributions in lipped and un-lipped channels in an attempt to isolate shear stresses acting on the section. Their

* Corresponding author.
E-mail addresses: luke.lapira15@imperial.ac.uk (L. Lapira), leroy.gardner@imperial.ac.uk (L. Gardner), a.wadee@imperial.ac.uk (M.A. Wadee).

https://doi.org/10.1016/j.tws.2022.110150
Received 25 May 2022; Received in revised form 30 July 2022; Accepted 13 September 2022
Available online xxxx
0263-8231/© 2022 The Author(s). Published by Elsevier Ltd. This is an open access article under the CC BY license (http://creativecommons.org/licenses/by/4.0/).

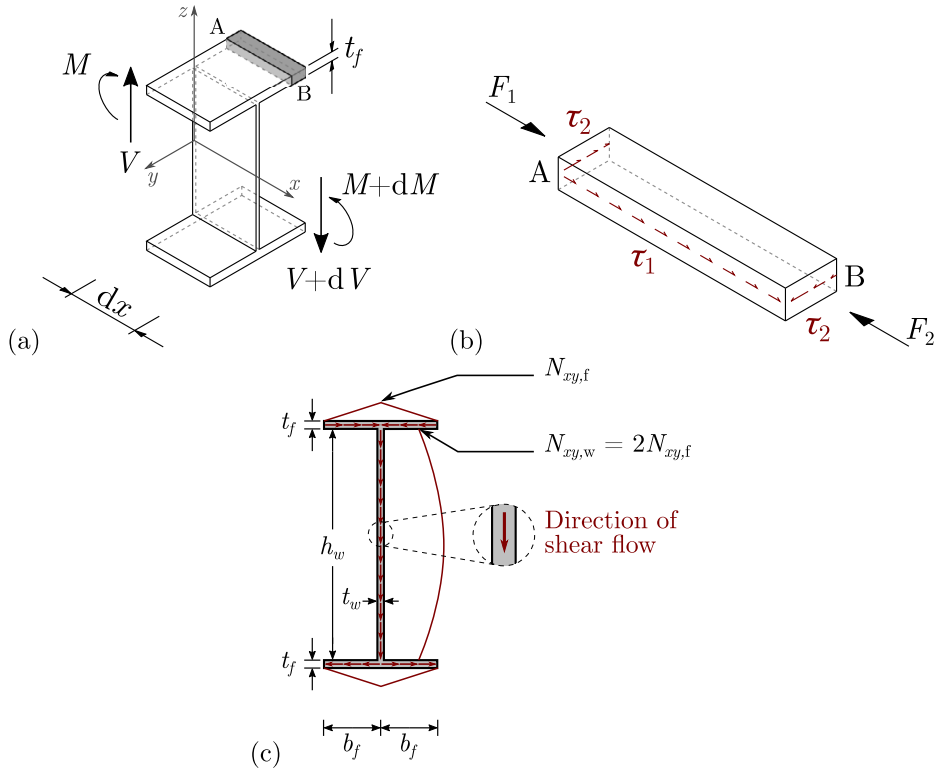


Fig. 1. (a) Free body diagram of I-section subjected to shear and bending forces; (b) a section of the flange to determine the shear stresses in the flange; (c) the resulting shear flow in the I-section, noting that the shear flow in the web $N_{xy,w}$ is twice the shear flow in each flange $N_{xy,f}$.

primary motivation was to develop shear buckling design provisions for use in the Direct Strength Method (DSM) [9]. Similar work has been conducted to determine the influence of corner bend radii on the overall cross-section buckling stress of cold-formed sections [10–12].

In the present article, formulae for evaluating the elastic local buckling stress of thin-walled I-sections subjected to shear stresses and a combination of shear and direct in-plane stresses, following the methodology in [4] are developed. The underlying concept of this approach is first introduced. The elastic local buckling stress of the both the web and flange of the I-section, under the shear stresses arising from the shear flow within the section in bending, is then examined in isolation, i.e. neglecting direct stresses. An FE study, exploring the influence of typical geometric parameters of welded I-sections, is used to calibrate closed-form predictive functions for the full cross-section buckling stress under shear. The results are compared to the current methodology adopted in EN 1993-1-5 [1], demonstrating that the proposed functions are significantly more accurate and reliable. Finally, the approach is extended to include cross-sections subjected to a combination of axial, bending and shear forces; again, the results are shown to be both accurate and reliable.

2. Concept

The conceptual framework used in this study is similar to that previously established in [4], and is recapitulated herein. The elastic buckling stress of a cross-section $\sigma_{cr,cs}$ lies within the bounds defined by the local buckling stress of the critical plates when isolated with simply-supported $\sigma^{SS}_{cr,p}$ and fixed $\sigma^{F}_{cr,p}$ boundary conditions along the commonly adjoined edges. The lower and upper bounds of the elastic buckling stress are defined as the lesser of the elastic buckling stress of the isolated web and flange plates with the respective boundary conditions thus:

$$\sigma^{SS}_{cr,p} = \min\left(\sigma^{SS}_{cr,w}, \sigma^{SS}_{cr,f}\right), \tag{1}$$

$$\sigma^{F}_{cr,p} = \min\left(\sigma^{F}_{cr,w}, \sigma^{F}_{cr,f}\right), \tag{2}$$

where the lower bound buckling stress $\sigma^{SS}_{cr,p}$ is the minimum shear buckling stress of the isolated plate (i.e. flange $\sigma^{SS}_{cr,f}$ or web $\sigma^{SS}_{cr,w}$) with simply-supported boundary conditions along the adjoined edges, while the upper bound buckling stress $\sigma^{F}_{cr,p}$ is the minimum buckling stress of the isolated plate (i.e. flange $\sigma^{F}_{cr,f}$ or web $\sigma^{F}_{cr,w}$) with fixed boundary conditions along the adjoined edges [4].

The lower and upper bound elastic buckling stresses are often defined by the same plate, but this condition is not necessary and may on occasion be defined by different plates. The elastic buckling stress of the cross-section lies between the established boundaries and is dependent on the relative restraint provided by the adjoining elements, as expressed through the interaction coefficient ζ. The concept is thus expressed algebraically:

$$\sigma_{cr,cs} = \sigma^{SS}_{cr,p} + \zeta\left(\sigma^{F}_{cr,p} - \sigma^{SS}_{cr,p}\right) \text{ where } 0 \le \zeta \le 1. \tag{3}$$

The extent of the element interaction is quantified by the coefficient ζ that defines the influence of the non-critical plates on increasing the elastic buckling stress of the critical plate beyond that associated with simply-supported boundary conditions. For cases where $\zeta = 0$, no element interaction occurs, thus Eq. (3) reduces to the elastic buckling stress of the critical isolated plate with simply-supported boundary conditions, whereas if $\zeta = 1$, Eq. (3) reduces to the buckling stress of the critical isolated plate with rotationally restrained boundary conditions. An important feature of the approach is that element interaction can arise even when the isolated cross-section plates have the same elastic buckling stress due to differences in the local buckling half-wavelengths of the isolated plates [4,13].

3. Stresses in I-sections under bending and shear

3.1. Shear stress in web and flange

It is well established that for I-sections subjected to shear forces, the shear flow in the web is equal to twice the shear flow in each flange at the web to flange junction as depicted in Fig. 1. To explain this

behaviour for the present context, a review of how shear stress develops in the flange of an I-section is offered. For clarity, subscripts of τ and σ are used throughout to distinguish whether the terms respectively relate to the shear or direct stresses.

Consider a simply-supported I-section beam subjected to a linearly varying moment M and constant shear force V, as shown in Fig. 1(a). From elementary beam theory, $V = \mathrm{d}M/\mathrm{d}x$. Consider further a free-body AB taken from the top flange of the I-section, shown in Fig. 1(b). The difference in the normal forces F_1 and F_2, acting on faces A and B of the free-body shown and caused by the changing moment along the beam, gives rise to a shear stress τ_1 which is necessary for the free-body AB to maintain equilibrium in the x-direction. This shear stress, in turn, gives rise to complementary shear stresses τ_2 on both faces A and B. It follows that while the value of τ_1 is constant along $\mathrm{d}x$, the complementary shear stress τ_2 varies linearly from a minimum value of zero at the free edge to a maximum value at the web to flange junction; this is represented in Fig. 1(c), where the arrows within the cross-section depict the shear flow within an I-section subjected to vertical shear force. Thus, the flanges of the I-section are subjected to a linearly varying shear stress along the edges of the free-body.

Therefore, to compare the shear stresses in the web and the flange, an appropriate adjustment is necessary to evaluate the critical element. This is performed by using the non-dimensional coefficients $\beta_{\tau,\mathrm{f}}$ and $\beta_{\tau,\mathrm{w}}$, established previously in [4] for normal stresses, but adapted herein to apply to the shear stresses in the flange and web respectively, as presented in Section 5,

$$\tau_{\mathrm{max,cs}} = \max\left(\tau_{\mathrm{max,f}}, \tau_{\mathrm{max,w}}\right), \tag{4}$$

$$\beta_{\tau,\mathrm{f}} = \frac{\tau_{\mathrm{max,cs}}}{\tau_{\mathrm{max,f}}} \geq 1, \tag{5}$$

$$\beta_{\tau,\mathrm{w}} = \frac{\tau_{\mathrm{max,cs}}}{\tau_{\mathrm{max,w}}} \geq 1, \tag{6}$$

where $\tau_{\mathrm{max,f}}$ and $\tau_{\mathrm{max,w}}$ are the largest shear stresses in the flange and web respectively, and $\tau_{\mathrm{max,cs}}$ is the maximum shear stress in the cross-section.

3.2. Finite element modelling

The numerical investigation presented in this study was conducted by means of Finite Element (FE) analysis of models developed within the commercial package Abaqus [14]. To ensure compatibility of the numerical results with previously established solutions developed using thin-plate theory [8,15–19], the 4-noded thin shell element with reduced integration and five degrees of freedom per node 'S4R5' available in the Abaqus library is used. A Linear Buckling Analysis (LBA) was used to determine the buckling coefficients of the following cases:

1. the isolated web-plate subjected to pure shear stress,
2. the isolated flange subjected to linearly varying shear stress,
3. the entire cross-section subjected to pure shear, and
4. the entire cross-section subjected to combined bending and shear.

In all analyses, the sections were meshed with 50 elements along the height of the web h_w. The number of elements across the flange and along the length of the section was varied such that a square element aspect ratio was maintained. This mesh was established following a mesh-convergence study, noting that the resulting buckling coefficient converged to within 1% of a mesh with 100 elements along the web width.

The loading and boundary conditions for all cases are depicted in Fig. 2, where the edges are enumerated and encircled, the corner nodes are enumerated and boxed, and the tables indicate free and restrained boundary conditions with values of '-' and 'R' respectively. For the isolated plates, boundary conditions indicated by 's/f' represent simply-supported or rotationally fixed $\left(\theta_x = \mathrm{R}\right)$ edges. For the full cross-section, the boundary conditions were carefully studied to ensure that the same set of boundary conditions could be used for cases of pure shear, direct stresses and combined loads. This was achieved by applying an *Equation constraint to the nodes along the supported flange edge, constraining their z-direction deflections to be equal to the deflections of the node at the respective web to flange junction. The parametric study was executed by varying the geometrical parameters outlined in Table 1; all studied I-sections were doubly-symmetric. The height h_w and thickness t_w of the web was fixed to 1000 mm and 2 mm respectively in all cases, and the sections were modelled using centre-line approximations in Abaqus. The parabolic distribution of the shear stresses along the depth of the web has been presently simplified to a state of pure shear stress, such that the results presented herein are consistent with previous work on shear buckling [8,16–19]. A preliminary comparative investigation found that the effect of this simplification on the derived shear buckling coefficients k_τ was negligible.

Table 1
Parameters varied to capture behaviour of cross-sections.

Parameter		Range of values
Web aspect ratio	a/h_w	[0.5–5.0]
Flange to web thickness	t_f/t_w	[0.1–10.0]
Flange width to web height	b_f/h_w	[0.1–0.5]
Direct stress ratio	ψ	[−1.0–1.0]

4. Buckling coefficients for isolated plates under shear stress

For plates subjected to direct stresses, the variation of the buckling coefficient with the plate aspect ratio is typically conservatively ignored and the minimum values are used, but it is overly conservative to ignore this variation for plates subjected to shear stress because webs are commonly stiffened at close intervals leading to plate aspect ratios close to unity. In this section, the numerical results of the buckling coefficients for isolated plate elements and full I-sections under shear stress are presented.

4.1. Internal plate subjected to pure shear stress

For rectangular plates subjected to pure shear stress, Timoshenko [17] derived, using the energy method, an expression for the elastic critical shear buckling stress $\tau_{\mathrm{cr,p}}$,

$$\tau_{\mathrm{cr,p}} = \frac{k\pi^2 E}{12\left(1-\nu^2\right)\left(h_w/t_w\right)^2}, \tag{7}$$

where E and ν are respectively the plate material Young's Modulus and Poisson's ratio, t_w and h_w are respectively the thickness and height of the plate, and k is the plate buckling coefficient that varies with loading, geometry and boundary conditions. Presently, k is distinguished between k_σ, when the element is loaded by direct stresses (ranging from compression to bending), and k_τ when the element is loaded in shear. In terms of the boundary conditions, the superscript 'SS' indicates that all edges of the plate are simply-supported, while the superscript 'F' denotes that the plate edges along the length a are rotationally fixed.

Southwell and Skan [15] solved for the buckling coefficient k_τ of long plates ($a/h_w \to \infty$) with all edges simply-supported ($k_\tau^{\mathrm{SS}} = 5.35$) and fixed ($k_\tau^{\mathrm{FF}} = 8.98$). Stein and Neff [16] solved the problem for simply-supported plates subjected to pure shear, showing how the minimum buckling coefficient k_τ^{SS} varies with varying plate aspect ratio a/h_w and converges to $k_\tau^{\mathrm{SS}} = 5.35$, as reported by Southwell and Skan. As the aspect ratio of the plates changes, the critical eigenmode shifts between a symmetric mode and an antisymmetric mode, resulting in a local maxima in k_τ in the vicinity of this transition. For practical purposes, the variation of k_τ with aspect ratio can be approximated by the function,

$$k_\tau^{\mathrm{SS}} = \begin{cases} 4 + 5.34\left(h_w/a\right)^2 & a/h_w < 1, \\ 5.34 + 4\left(h_w/a\right)^2 & a/h_w \geq 1, \end{cases} \tag{8}$$

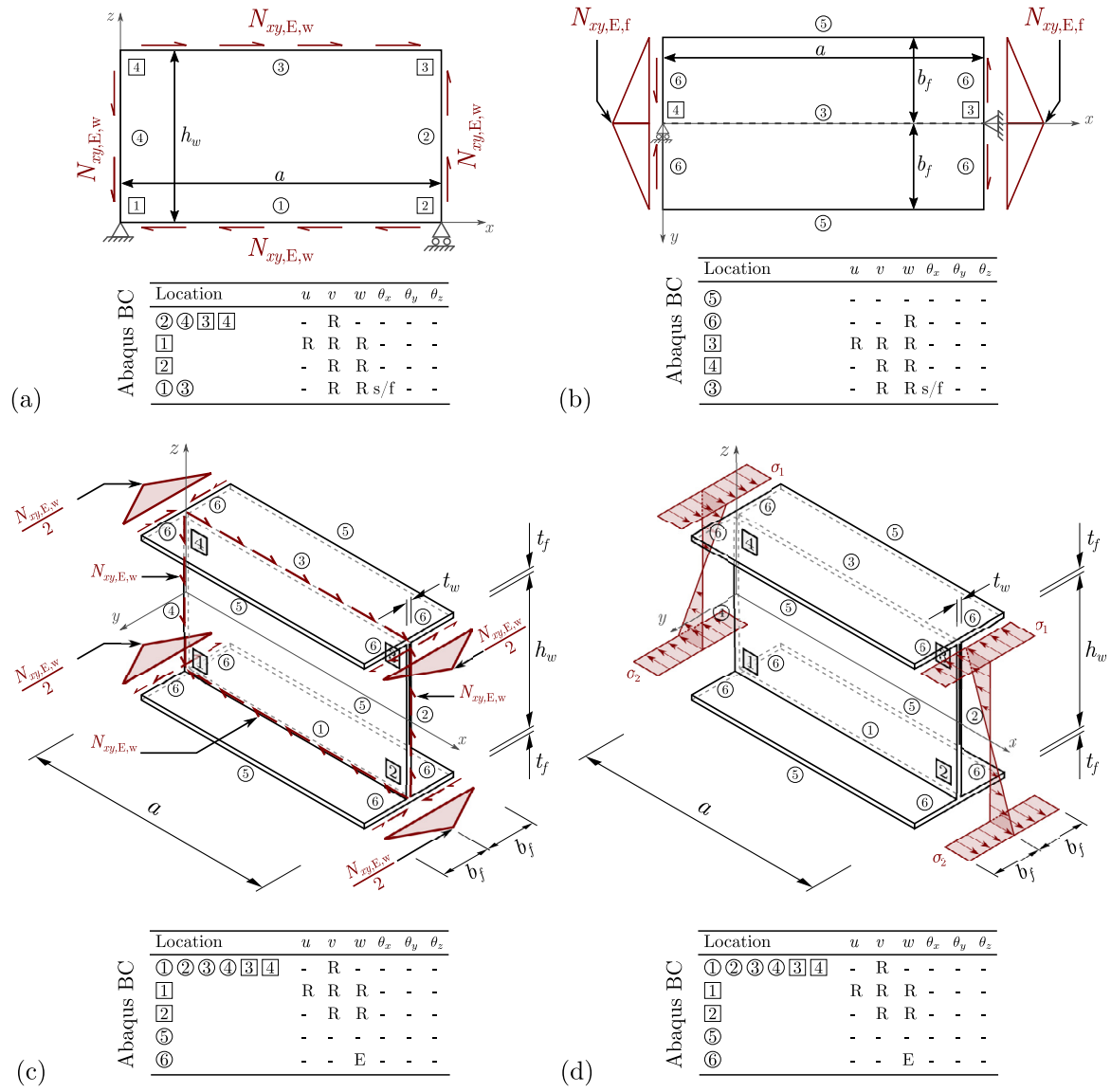


Fig. 2. Abaqus loading and boundary conditions for: (a) isolated web plate subjected to pure shear stress; (b) isolated flange subjected to linearly varying shear; (c) full cross-section subjected to shear stress; (d) full cross-section subjected to bending stress. Labels '-' and 'R' indicate free and restrained degrees of freedom respectively, 'E' represents an equation constraint and 's/f' change between free and fixed respectively, depending on whether the plate flexural boundary conditions along that edge are simply-supported or fixed.

which is provided in design codes, including EN 1993-1-5 [1], and is depicted in Fig. 3(a). The function in Eq. (8) represents a lower-bound approximation to the variation of k_τ^{SS} with a/h_w, especially at the transition between symmetric and anti-symmetric buckling modes. Solutions have also been derived for plates subjected to pure shear with various edge boundary conditions by Iguchi [20] and Cook and Rockey [18]. The solutions from the latter are generally accepted as being the more accurate, since Iguchi ignored the anti-symmetric buckling mode when determining the buckling coefficients k_τ [19]. Simplified expressions for k_τ^F as it varies with a/h_w are presented by Lee et al. [8] as:

$$k_\tau^F = \begin{cases} 5.34\left(h_w/a\right)^2 + 2.31\left(h_w/a\right) - 3.44 + 8.39\left(a/h_w\right) & a/h_w < 1, \\ 8.98 + 5.61\left(h_w/a\right)^2 - 1.99\left(h_w/a\right)^3 & a/h_w \geq 1, \end{cases} \tag{9}$$

and are shown in Fig. 3(a).

For internal plates (i.e. those with out-of-plane translational support along all four edges) subjected to pure shear, the results from the FE models are compared with the approximations in Eqs. (8)–(9). The FE results closely follow the analytical predictions within the range of parameters considered, as shown in Fig. 3(a).

4.2. Outstand plates subjected to linearly varying shear stresses

While the problem for the internal plates subjected to pure shear stress is well defined and researched, to the authors best knowledge, there is no published work that examines the behaviour of outstand plates (i.e. those with three translationally supported edges, with the fourth free) subjected to linearly varying shear stresses that develop in the flanges of cross-sections. Based on the conditions depicted in Fig. 2(b), results are established herein to enable predictions of the buckling coefficients k_τ of outstand plates under shear. The model depicted in Fig. 2(b) is based on the explanation offered in Section 3.1, where although the web is under pure shear, the outstand flanges are subjected to a linearly varying complementary shear stress that varies from a minimum value of zero at the free edge to a maximum value at the web-to-flange junction, as shown in Fig. 1(c).

While the web of the cross-section can be studied in isolation in a state of self-equilibrated pure shear, the individual flange plates,

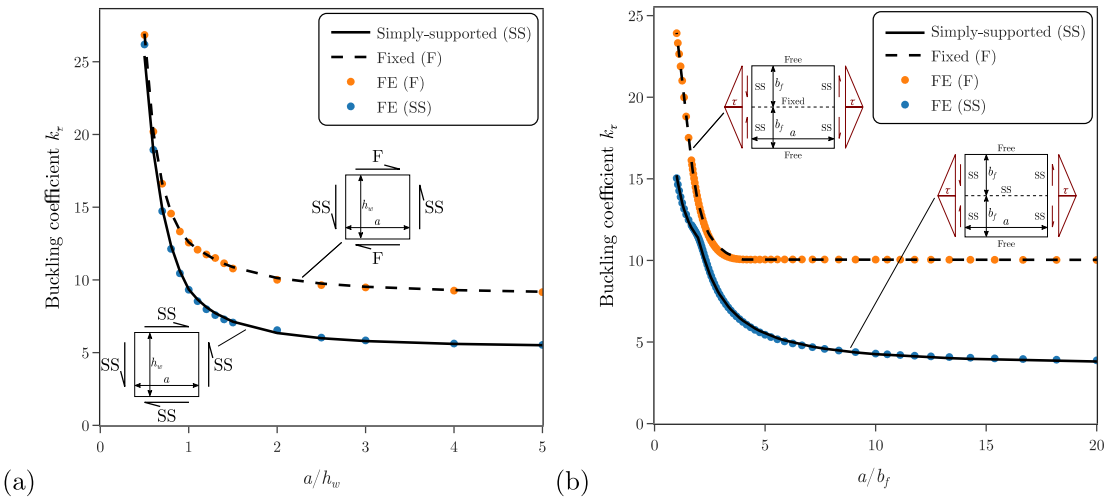


Fig. 3. Buckling coefficient k_τ for (a) internal plates subjected to pure shear stress and (b) outstand plates subjected to linearly varying shear stress with simply-supported and fixed boundary conditions along the adjoined edges. Boundary conditions for (a) and (b) are depicted in Fig. 2(a)–(b), respectively, and expressions for k_τ are provided in Table 2.

which are subjected to the shear stresses described, would not be in equilibrium if studied in isolation. To achieve equilibrium, it would be necessary to introduce a linearly varying force, such as that introduced by means of a linearly varying moment in the free-body shown in Fig. 1(a). This has been found by other researchers also attempting to isolate the elastic buckling stress of full cross-sections subjected to shear [2,21]. Despite this shortcoming, the loading conditions shown in Fig. 2(b) are suitable for representing the shear effects on the flanges and hence determining the shear buckling coefficient for isolated flange plates, while equilibrium is provided by the FE model boundary conditions [21].

In the FE models, both half-flange outstand plates were modelled to reduce the imbalance in the applied forces, thereby equilibrating the forces that the boundary conditions were required to resist. The boundary conditions modelled at the intersection of the two plates are shown in Fig. 2(b) and ensure overall equilibrium. Edges ③ and ⑥ are restrained from displacing out-of-plane in the z-direction, representing simple supports along those edges, while edge ⑤ is left free. A non-uniform shear stress resultant is applied to the flange along edge ⑥ in the directions shown in Fig. 2(b), varying from zero at the tips to a peak value of $N_{xy,\mathrm{E,f}}$ at the web-to-flange junction. The value of $N_{xy,\mathrm{E,f}}$ is defined thus:

$$N_{xy,\mathrm{E,f}} = \frac{\pi^2 E t_f^3}{12\left(1-\nu^2\right) b_f^2}, \tag{10}$$

where t_f is the thickness of the flange and b_f is the width of the flange outstand. By defining $N_{xy,\mathrm{E,f}}$ in this manner, the resulting eigenvalue from the LBA in Abaqus is equal to the critical buckling factor for the simply-supported flange under shear stress k_τ. FE results were generated for a practical range of flange aspect ratio values a/b_f varying from 1 to 50, considering edge ③ to be either simply-supported or rotationally fixed. The results from the FE analyses are shown in Fig. 3(b), with the associated proposed functions for predicting k_τ presented in Table 2.

5. I-sections subjected to shear stress

In the current section, expressions for determining the full cross-section elastic local buckling stress of I-sections subjected to shear stress are presented. Having established the local buckling stress of the isolated plates with simply-supported and fixed boundary conditions, the interaction coefficient ζ_τ needs to be determined for the cross-sections analysed within the parametric study. In a similar manner to the work on cross-sections subjected to direct stresses [4], the parameter ϕ_τ, where:

$$\phi_\tau = \frac{\beta_{\tau,\mathrm{f}}\tau^{\mathrm{SS}}_{\mathrm{cr,f}}}{\beta_{\tau,\mathrm{w}}\tau^{\mathrm{SS}}_{\mathrm{cr,w}}}, \tag{11}$$

delineates whether the simply-supported lower bound buckling stress is defined by the flange $(\phi_\tau < 1)$, or by the web $(\phi_\tau \geq 1)$.

5.1. I-section buckling coefficients

To determine the buckling coefficients of I-sections subjected to pure shear, the model depicted in Fig. 2(c) was analysed in the parametric study. The web was loaded in a state of pure shear such by applying shear loads along the web edges with a magnitude of $N_{xy,\mathrm{E,w}}$ defined as:

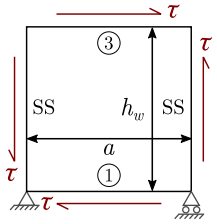
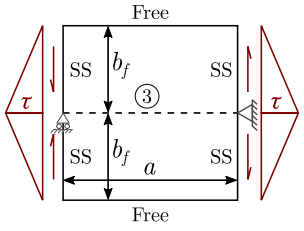
$$N_{xy,\mathrm{E,w}} = \frac{\pi^2 E t_w^3}{12\left(1-\nu^2\right) h_w^2}, \tag{12}$$

where t_w and h_w are respectively the thickness and height of the web. The flanges were loaded along the supported edges with a linearly varying shear stress resultant equal to half the shear flow in the web at the web-to-flange junction (i.e. $N_{xy,\mathrm{E,w}}/2$), as discussed in Section 3.1. In this manner, the eigenvalue from the LBA in Abaqus was equal to the buckling coefficient k_τ of the cross-section. As for the FE models of the isolated flange plates, the FE models of the full cross-sections in shear also required the equilibrating forces to be resisted by the boundary conditions. The adopted loading conditions, shown in Fig. 2(c), are nonetheless considered to be suitable for isolating the shear from the bending effects for the purpose of identifying the pure shear buckling stress and corresponding mode of the cross-section [21].

The results from the parametric FE study are plotted in Fig. 4, and are classified into two groups for (a) web-critical and (b) flange-critical cases. In each of the subplots, the black lines depict the upper and lower boundaries for the cases using the expressions summarised in Table 2. As discussed in Section 2, the upper and lower bounds need not be provided by the same plate. Therefore, the results have each been categorised into one of four permutations of the lower and upper bounds, as detailed in Table 3.

Considering first the web-critical 'Case WW' sections, where the upper and lower bound are both defined by the isolated web plate with fixed and simply-supported boundary condition respectively, the results, shown in Fig. 4(a), lie within the boundaries established in Table 2. For web aspect ratios $a/h_w < 1$, the FE buckling coefficient exceeds the established upper bound limit for a few of the results,

Table 2
Summary of expressions for the buckling coefficient k_τ for internal and outstand plates subjected to shear stresses.

Stress conditions	Boundary	Buckling coefficient		Ref.
Internal plates 	①, ③ SS	$k_\tau = 4 + 5.34\left(h_w/a\right)^2$	$a/h_w < 1$	[17]
		$k_\tau = 5.34 + 4\left(h_w/a\right)^2$	$a/h_w \geq 1$	[17]
	①, ③ F	$k_\tau = -3.44 + 5.34\left(h_w/a\right)^2 + 2.31\left(h_w/a\right) + 8.39\left(a/h_w\right)$	$a/h_w < 1$	[8]
		$k_\tau = 8.98 + 5.60\left(h_w/a\right)^2 - 1.99\left(h_w/a\right)^3$	$a/h_w \geq 1$	[8]
Outstand plates 	③ SS	$k_\tau = 9.22 + 6/\left(a/b_f\right)^{3/2}$	$a/b_f \leq 2$	[a]
		$k_\tau = 3.56 + 22/\left(a/b_f\right)^{3/2}$	$a/b_f > 2$	[a]
	③ F	$k_\tau = 35.64 - 11.7\left(a/b_f\right)$	$a/b_f \leq \frac{5}{3}$	[a]
		$k_\tau = 9.58 + 30.34/\left(a/b_f\right)^3$	$a/b_f \leq 4$	[a]
		$k_\tau = 10 + 2.54/\left(a/b_f\right)^3$	$a/b_f > 4$	[a]

[a]Proposed functions from present analyses.

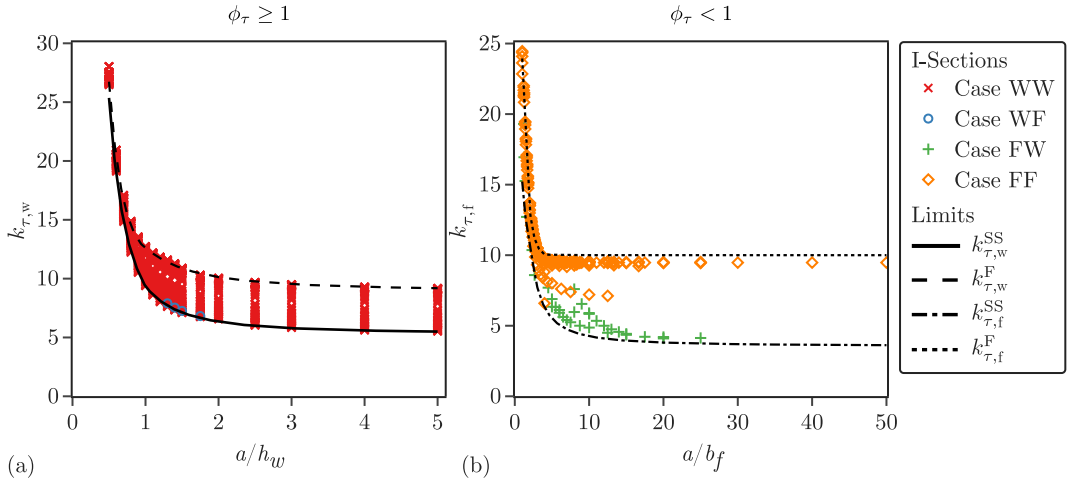


Fig. 4. Results of the parametric FE analysis classified as (a) web-critical cases ($\phi \geq 1$) and (b) flange-critical cases ($\phi < 1$), where Cases WW, WF, FW and FF are defined in Table 3.

Table 3
The four cases of lower and upper bound limits defined by the critical web or flange.

Case	Lower bound	Upper bound
WW	Web	Web
WF	Web	Flange
FW	Flange	Web
FF	Flange	Flange

indicating that the resulting predictions are very slightly conservative in this region. For the flange-critical 'Case FF' sections, the upper and lower bound limits are defined by the isolated flange plate with fixed and simply-supported boundary condition respectively. The FE data shown in Fig. 4(b) demonstrate that the results lie within the boundaries established in Table 2, thereby confirming the validity of the adopted approach.

For 'Case WF', the validity of the upper bound cannot be assessed from Fig. 4(a) since the upper bound should be defined by the isolated flange with fixed boundary conditions. Thus, the results are considered separately in Fig. 5(a)–(b). In Fig. 5(a), the results for 'Case WF' are plotted using the web-related parameters, and should therefore lie above the limit shown. In Fig. 5(b), the buckling coefficients k_τ are calculated in terms of the flange geometry $k_{\tau,\mathrm{f}}$ and should lie below the limit shown. It is emphasised that the two subplots represent two distinct interpretations of the same results. A similar analysis is necessary for 'Case FW', the results of which are shown in Fig. 5(c)–(d), demonstrating the suitability of the established bounds.

5.2. Formulae for determining the cross-section buckling stress

Having established the lower and upper bound limits, and determined the elastic critical buckling stress under shear of the cross-sections, the buckling interaction coefficient under shear $\zeta_{\tau,\mathrm{FE}}$ is back-calculated for each of the cross-sections in the parametric study using the expression:

$$\zeta_{\tau,\mathrm{FE}} = \frac{\tau_{\mathrm{cr,cs}} - \tau_{\mathrm{cr,p}}^{\mathrm{SS}}}{\tau_{\mathrm{cr,p}}^{\mathrm{F}} - \tau_{\mathrm{cr,p}}^{\mathrm{SS}}}. \tag{13}$$

The results are analysed separately for web-critical sections ($\phi_\tau \geq 1$) and flange-critical sections ($\phi_\tau < 1$). When $\phi_\tau = 1$, the web and flange

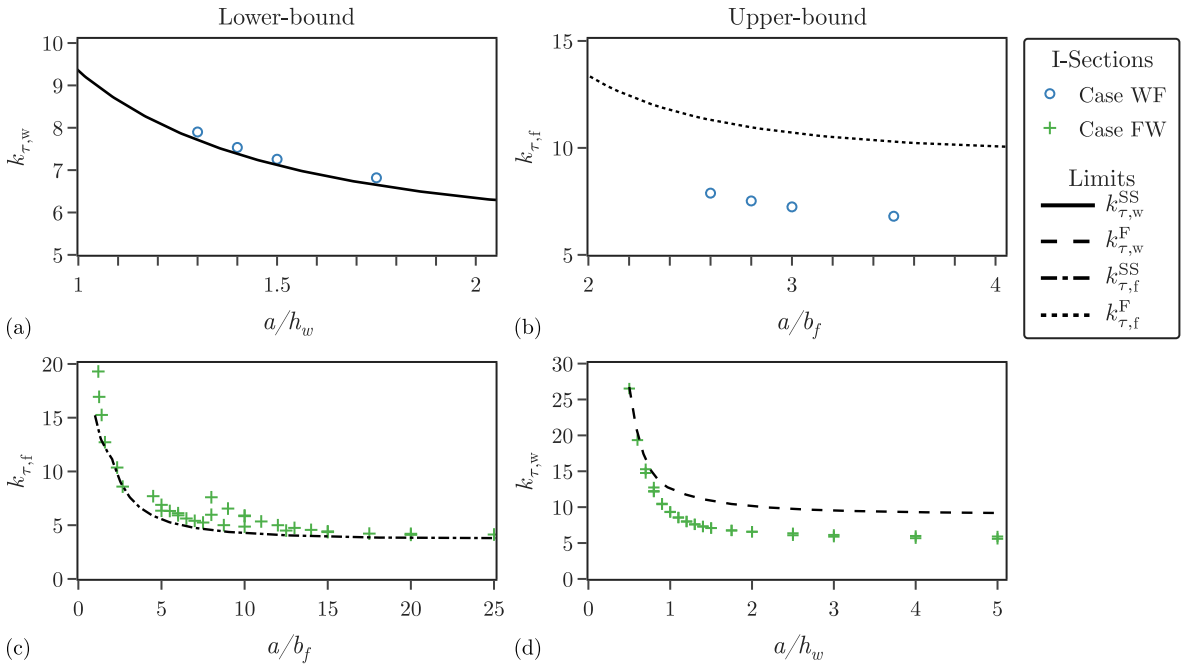


Fig. 5. Case WF results within the (a) lower and (b) upper bounds; Case FW results within the (c) lower and (d) upper bounds.

are equally susceptible to buckling, and $\zeta_\tau = 0$ might be expected in such scenarios. However, this is not necessarily the case since an increase in the buckling stress of the cross-section can also occur if the buckling modes of the isolated plates have different wavelengths resulting in $\zeta_\tau > 0$ at $\phi_\tau = 1$ [4,13].

The variation of the back-calculated ζ_τ coefficients with ϕ_τ for I-sections subjected to pure shear stress are plotted in Figs. 6–8. The web-critical results follow a $(1 - 1/\phi_\tau)$ relationship, which implies a higher interaction factor ζ_τ as $1/\phi_\tau$ approaches 0, i.e. when the flange buckling stress is much larger than the web buckling stress. When the elastic buckling stress of the simply-supported web is much higher than that of the flange, $\phi_\tau \to 0$ and hence the back-calculated ζ_τ results approach unity. This echoes the results for sections subjected to direct stresses [4].

5.2.1. Web-critical sections

The web-critical sections are those where the lower bound (simply-supported) limit is defined by the elastic buckling stress of the web, i.e. Cases WW and WF. In Fig. 6(a), the back-calculated $(1 - \zeta_\tau)$ values are plotted against the inverse elastic buckling stress ratio $1/\phi_\tau$, to determine the key parameters that drive the relationship. Considering $1/\phi_\tau$ is instructive here since, for a large number of the cross-sections that are web-critical, the isolated flange buckles at a much higher stress than the isolated web and therefore ϕ_τ can reach very large values. By considering $1/\phi_\tau$, on the other hand, the results are concentrated in the range $0 < 1/\phi_\tau \leq 1$, facilitating the prediction of ζ_τ. In Fig. 6(a), there is a clear trend between ϕ_τ and ζ_τ, indicating the applicability of ϕ_τ as a governing parameter for the prediction. There is, however, a large scatter in the results which can be reduced by the introduction of geometric parameters, particularly the flange to web thickness ratio t_f/t_w and the flange width to web height ratio b_f/h_w, as shown in Fig. 6(b).

It is further noted that when the web panel aspect ratio $a/h_w < 1$ the degree of scatter is considerably greater than for the remaining cross-sections with $a/h_w \geq 1$, as shown in Fig. 7. Although the expression does not accurately predict ζ_τ when $a/h_w < 1$, it is noted that the error is safe-sided, in the sense that the prediction underestimates the degree of interaction. Furthermore, when $a/h_w < 1$ the difference between the lower and upper bound critical stress of the panels is numerically small, as can be seen in Fig. 4(a). Therefore, the influence of an inaccurate prediction of ζ_τ in these cases has a diminished impact on the accuracy of the final prediction for the cross-section elastic buckling stress $\tau_{cr,cs}$.

5.2.2. Flange-critical cross-sections

Flange-critical cross-sections are defined as those where the elastic buckling stress of the simply-supported flange is lower than that of the simply-supported web, i.e. Cases FW and FF defined in Table 3. In practice, such sections rarely occur, because the necessary proportions (thick, shallow web and thin, wide flanges) are not typically structurally efficient. In fact, in the parametric study, flange-critical sections occur only when the flange to web thickness ratio $t_f/t_w < 1$, which tend to reduce their practical significance. The variation of ζ_τ with ϕ_τ for the flange-critical cases is shown in Fig. 8(a), demonstrating once more the suitability of ϕ_τ as a controlling parameter to predict the interaction coefficient ζ_τ. The buckling mode of a typical flange-critical cross-section in shear is shown in Fig. 8(b). The predictive function has been limited to $\zeta_\tau \leq 0.9$ to ensure that the majority of the predictions are safe-sided.

5.3. Evaluation of interaction formulae

The formulae to predict the cross-section interaction coefficient ζ_τ for I-sections subjected to shear stresses are summarised in Table 4. The proposed functions are evaluated by plotting normalised frequency distributions for both the full-cross-section elastic shear buckling stress calculated using ζ_τ and the elastic shear buckling stress of the isolated critical plate relative to the elastic shear buckling stress of the full cross-section as obtained from the FE model. These are shown in Fig. 9 for (a) the web-critical cases, (b) the flange-critical cases and (c) all the results. Predicted values less than 1 on the abscissa are safe-sided, while a lower Coefficient of Variation (CoV) indicates that the consistency of the predictions is high.

From the 1360 samples examined in the FE analyses, 1078 were web-critical sections and the remaining 282 were flange-critical sections. For the flange-critical sections, the mean ratio of the predicted full cross-section shear buckling stress to that determined from the FE

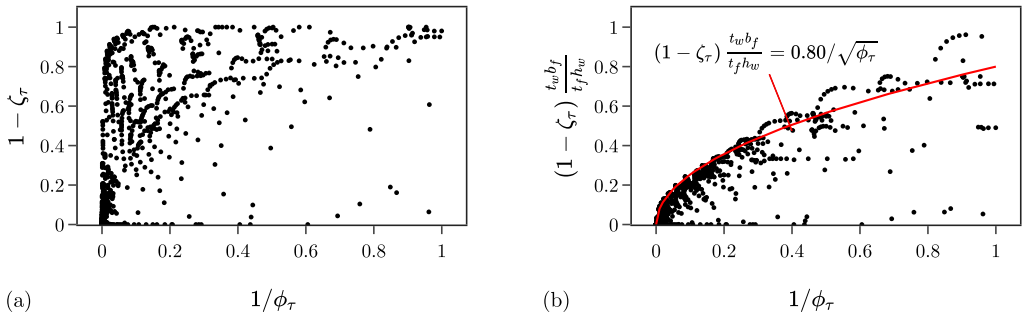


Fig. 6. Web-critical I-sections subjected to pure shear stress: (a) scatter in back-calculated interaction coefficients ζ_τ and (b) reduced scatter and proposed predictive function incorporating the geometric ratios t_f/t_w and b_f/h_w.

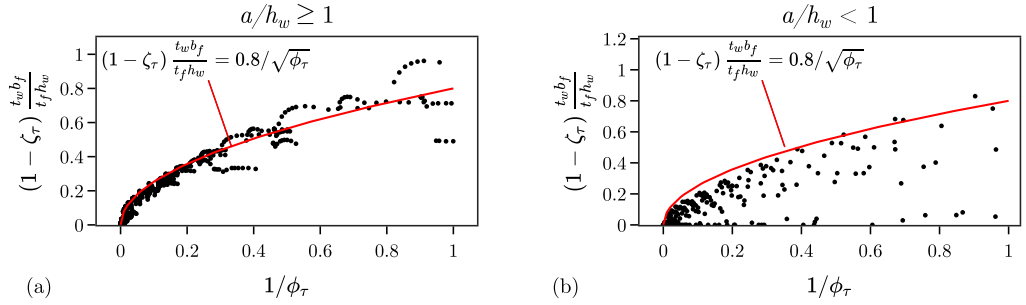


Fig. 7. Relationships between interaction function ζ_τ for web-critical I-sections subjected to pure shear stress versus the web aspect ratio a/h_w where: (a) $a/h_w \geq 1$ and (b) $a/h_w < 1$.

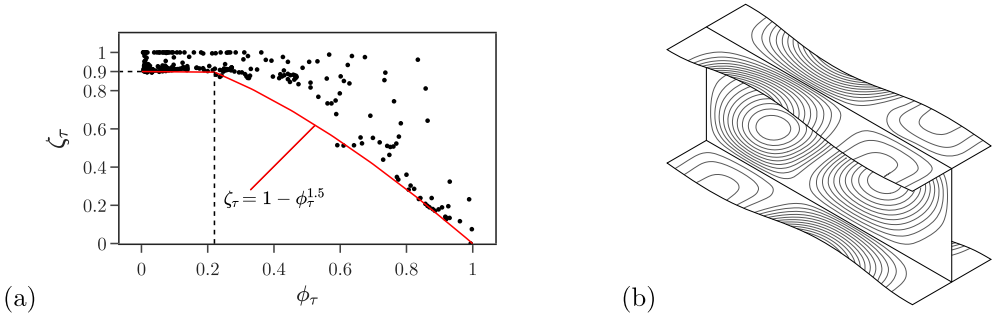


Fig. 8. (a) Variation of ζ_τ with ϕ_τ for flange-critical I-sections subjected to pure shear stress together with the predictive function; (b) Depiction of buckled shape in a flange-critical cross-section with $\phi_\tau = 0.66$ and $\zeta_\tau = 0.55$.

Table 4
Summary of simplified expressions for ϕ_τ, ϕ_σ and interaction coefficient ζ for I-sections subjected to different loads, where $0 \leq \zeta \leq 1$.

Load case		Ref.	ζ – flange-critical ($\phi < 1$)	ζ – web-critical ($\phi \geq 1$)
Shear	τ	[a]	$1-\phi_\tau^{1.5} \leq 0.9$	$1-\left(\frac{0.8}{\sqrt{\phi_\tau}}\frac{t_f}{t_w}\frac{h_w}{b_f}\right)$
Compression & major-axis bending	σ	[4]	$0.15\frac{t_f}{t_w}\phi_\sigma \geq \frac{t_w}{t_f}\left(0.4-0.25\phi_\sigma\right)$	$\frac{t_f}{t_w}\left(0.45-\frac{0.3}{\phi_\sigma^2}\right)$

[a]Proposed functions.

model is 0.97, with a CoV of 0.03. The flange-critical cases are underestimated by a significant margin if element interaction is ignored, with a mean prediction of 0.66 and a CoV of 0.23.

For the web-critical sections, the mean predicted full cross-section shear buckling stress is 0.95 of the FE results, with a CoV of 0.05. The results indicate a considerable improvement over the predictions that ignore element interaction, as is current practice in international design codes such as EN 1993-1-5 [1], which have a mean predicted-to-FE ratio of 0.83 with a CoV of 0.15. The FE results are over-predicted by the proposed formulae in fewer than 2% of the analysed cases. Evaluating the performance of the proposed functions for the web-critical sections against the predictions ignoring element interaction, the predicted buckling stress increases by a maximum value of 54%, with an average increase of 17%. When comparing the normalised frequency distribution plots, the isolated plate predictions are significantly more scattered than the proposed functions, further demonstrating that plate element interaction should not be ignored.

Considering the above analysis, the proposed functions are deemed to be highly effective in predicting the elastic buckling stress of full I-section profiles under shear. Since the proposed functions have been

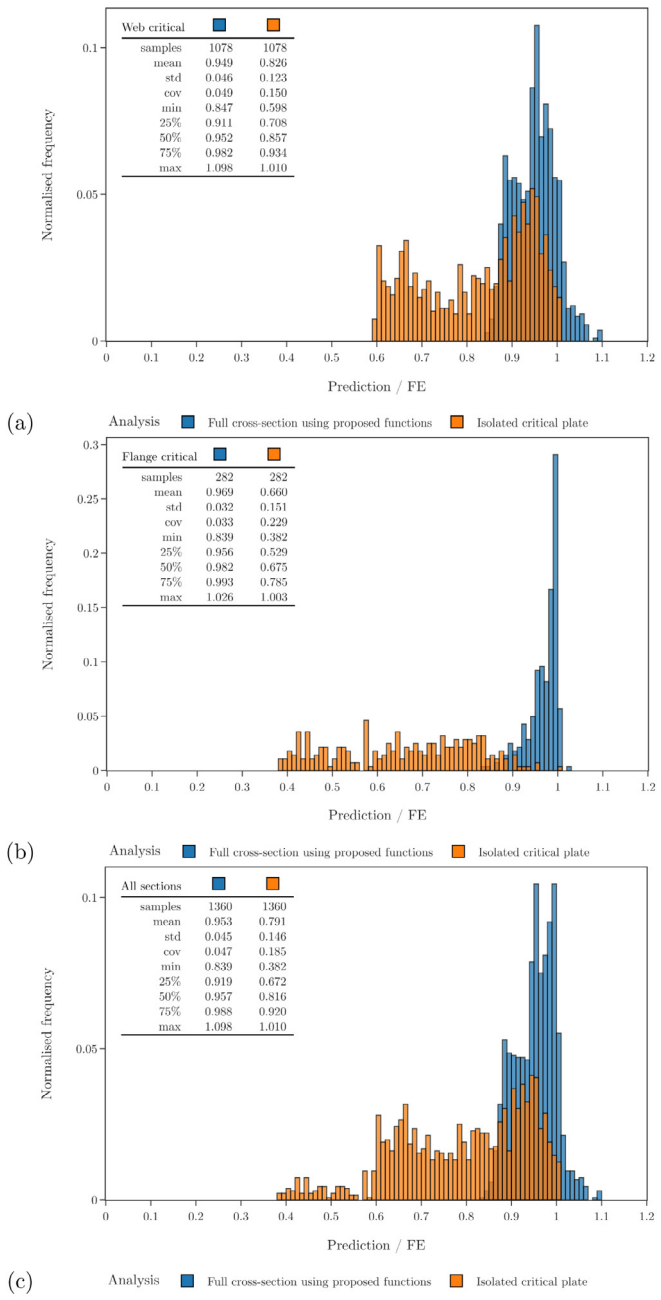


Fig. 9. Normalised frequency distributions, comparing the predicted buckling stresses of the cross-section using the proposed functions (blue) with the response ignoring element interaction (orange), where the critical isolated plate is (a) web-critical and (b) flange-critical. In (c) the normalised frequency distributions includes all cross-sections that have been analysed. (For interpretation of the references to colour in this figure legend, the reader is referred to the web version of this article.)

formulated based on FE analyses performed within the parametric range described in Table 1, the recommended scope of application of the model is also limited to this range. Further investigation could be conducted to explore a wider range of cross-section proportions and I-section geometries, but this is left for future work.

6. Buckling under combined shear and direct stresses

As demonstrated in Section 4.2, shear stresses develop in cross-sections to compensate for an imbalance in direct stresses along the member length, and therefore cannot practically occur in isolation. The buckling stress of cross-sections subjected to a combination of direct and shear stresses is thus investigated. The behaviour of the plates in isolation is considered first, before presenting the results of a parametric study on full cross-sections.

6.1. Buckling stress of isolated plates under combined loads

The results for the elastic buckling stress of isolated plates under combined direct and shear stresses are typically evaluated using normalised interaction curves [19,22], as shown in Fig. 10. In the curves shown, the values along the abscissa are the shear buckling stress of the plate under combined loading normalised by the elastic buckling stress of the plate under pure shear (τ/τ_{cr}), while the values along the ordinate are the direct buckling stress of the plate under combined loading normalised by the elastic buckling stress of the plate under pure direct stress (σ/σ_{cr}). The direct stresses applied to the plates are varied from pure compression to pure bending by changing the ratio of the direct stresses $\psi = \sigma_1/\sigma_2$, which are depicted in Fig. 2(d). Thus, the direct elastic buckling stress σ_{cr} on the ordinate axis changes for different values of ψ.

For a given plate, the interaction curves are evaluated by simultaneously applying the shear and direct stresses depicted in Fig. 2(c)–(d). The applied stresses are modified in accordance with the following expression:

$$M_1 \frac{\sigma}{\sigma_{FE}} + M_2 \frac{\tau}{\tau_{FE}} = 1 \tag{14}$$

where M_1 and M_2 are coefficients within the range $[0, 1]$, while σ_{FE} and τ_{FE} are the stresses applied to the FE model when each case is considered independently, such that the resulting eigenvalue from the LBA is equal to the buckling coefficient k. Simply put, the values of M_1 and M_2 are combined such that 11 load-cases for each plate under a particular (τ, σ) stress combination are studied thus:

$$(M_1, M_2) = [(1.0, 0.0), (0.9, 0.1), (0.8, 0.2), \ldots (0.0, 1.0)]. \tag{15}$$

The resulting eigenvalues from the FE analyses were then used to scale the results from the origin, resulting in the interaction plots shown in Fig. 10. Such interaction plots are often represented by a simplified relationship [23,24], such as that given in Eq. (16),

$$\left(\frac{\sigma}{\sigma_{cr}}\right)^p + \left(\frac{\tau}{\tau_{cr}}\right)^2 = 1, \tag{16}$$

where p changes with ψ.

Stowell and Schwartz [25] examined the case of plates subjected to combined shear and compression ($\psi = 1$), determining that setting the exponent $p = 1$ was suitable for such cases. Way [26] studied the case of simply-supported plates subjected to combined shear and bending ($\psi = -1$), examining the influence of plate aspect ratio a/h_w on the interaction curve within the range $0.5 \leq a/h_w \leq 1.0$. Way observed that the interaction curves for plates with different aspect ratios lay within a narrow zone, and thus a single interaction curve with $p = 2$ was found to provide a sufficiently accurate approximation to the observed behaviour. The two bounds of $p = 1$ when $\psi = 1$ and $p = 2$ when $\psi = -1$ have therefore been established based on previous research. The authors have not however found previous interaction expressions in which the exponent p is defined as a function of the stress ratio ψ. Using the FE results for the isolated plates, values for p that minimise the scatter of the FE results with respect to ψ have been determined thus:

$$p = \begin{cases} 1 - \psi^3 & -1 \leq \psi \leq 0, \\ 1 & 0 < \psi \leq 1. \end{cases} \tag{17}$$

The performance of this function is demonstrated for 6 separate values of ψ in Fig. 10, where the black curves represent the previously established boundaries [25,26], the 'o' and '×' markers are the FE results for the plates with simply-supported and fixed edges respectively,

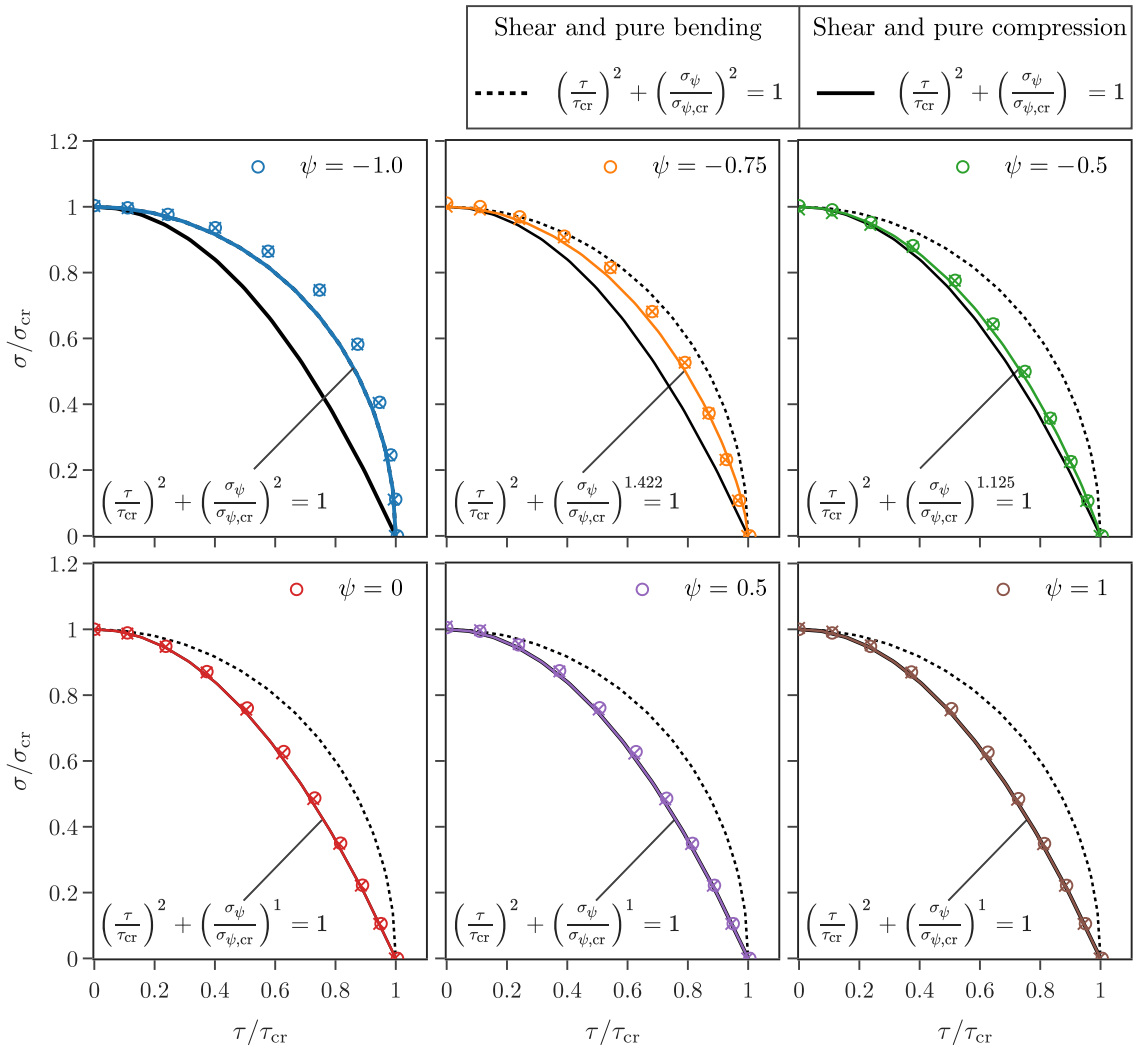


Fig. 10. Interaction plots for isolated plates subjected to combined shear and direct stress with $\psi = -1,\ -0.75,\ -0.5,\ 0,\ 0.5$ and 1 as indicated. The black lines are the limits established in the literature for plates simultaneously loaded under shear and compression (solid line) or shear and bending (dashed line). The coloured lines represent the interaction relationship given in Eq. (16) with the proposed values of the exponent p from Eq. (17). Individual points marked are from the FE solutions of the simply-supported plates (∘) and fixed plates (×). (For interpretation of the references to colour in this figure legend, the reader is referred to the web version of this article.)

while the coloured curves are the predicted interaction expressions using the values of p from Eq. (17). The interaction function in Eq. (16) is shown to be accurate for both simply-supported and fixed edged plates under combined shear and direct stress.

6.2. Buckling of I-sections under combined shear and direct stresses

The elastic buckling stress of full cross-sections under combined shear and direct stresses is evaluated using the same methodology described for isolated plates in Section 6.1. The FE results are limited to I-sections with $t_f/t_w \geq 1$, such that the models lie within the recommended range of applicability of the expressions established by Gardner et al. [4] for I-sections subjected to direct stress. To avoid impractical geometries, for the cross-sections with $b_f/h_w = 0.5$, values of $t_f/t_w > 2$ were not considered. The buckling stresses of the cross-sections are again bounded by the elastic buckling stress of the critical plate elements, which may differ by load case. For instance, a cross-section may be web-critical under shear but flange-critical under direct stresses. From the FE parametric study that is limited to I-sections with $t_f/t_w \geq 1$, there are no cross-sections that are flange-critical in shear. This simplifies the remaining permutations to cross-sections being web-critical under shear $(\phi_\tau \geq 1)$, and a possibility of the cross-sections being either web-critical $(\phi_\sigma \geq 1)$ or flange-critical $(\phi_\sigma < 1)$ under direct stresses.

Typical results from the FE analyses are shown in Fig. 11 for I-sections with $a/h_w = 5$ under combined shear and direct stresses with (a) $\psi = 1$ (pure compression), (b) $\psi = 0$ and (c) $\psi = -1$ (pure bending). From Fig. 11 it can be deduced that for each of the three cases depicted, the elastic buckling stress of the full cross-section subject to combined shear and direct stresses lie within the bounds defined in Section 2. Furthermore, as ψ changes from -1 to 0, the interaction shifts from a near perfect quadrant of a circular arc to a flatter response as expected from the change in the predicted exponent p. The bending solutions in Fig. 11(c) are noted to lie beyond the upper limit for a number of the FE models. This is presently attributed to the limit of the exponent p being equal to 2 for sections subject to pure bending regardless of the aspect ratio of the web panel, whereas it has been shown by Way [26] that this exponent changes slightly with aspect ratio.

6.3. Calculation of full cross-section buckling stress under combined loading

The elastic buckling stress of the full cross-section under combined shear and direct stresses is evaluated using the relationship established in Eq. (16). This requires first determining the elastic buckling stresses of the full cross-section under pure shear $\tau_{cr,cs}$ and only direct stresses $\sigma_{cr,cs}$ using the methodology described in Section 5 and in [4] respectively. Since the value of ψ is known, the value of p can be easily

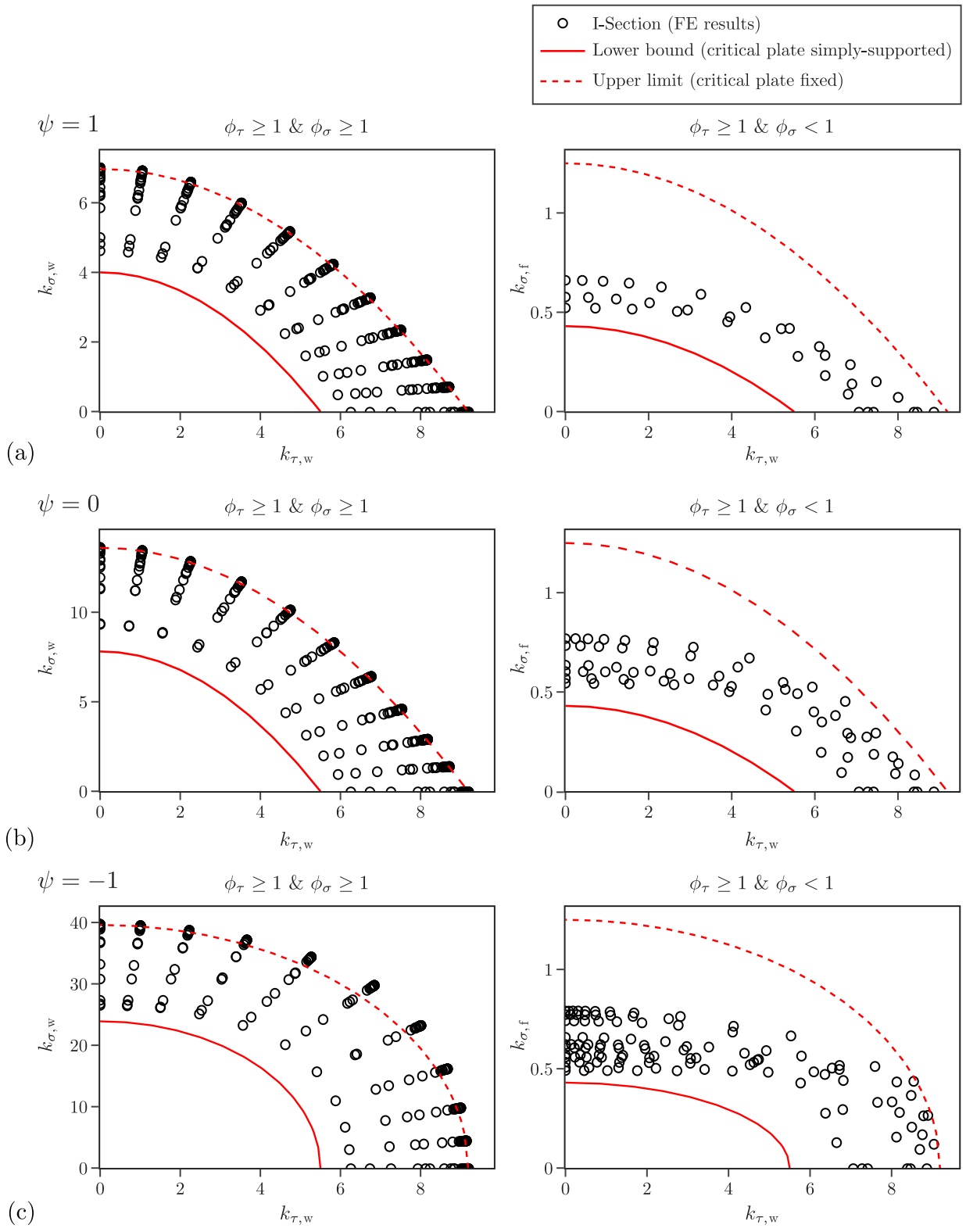


Fig. 11. Interaction of buckling coefficients k_σ and k_τ for cross-sections with $a/h_w = 5$ subjected to combined shear and direct stress where (a) $\psi = 1$ (pure compression), (b) $\psi = 0$ and (c) $\psi = -1$ (pure bending). Results on the left-hand side are web critical under direct stress ($\phi_\sigma \geq 1$) and results on the right-hand side are flange critical under direct stress ($\phi_\sigma < 1$); all results are web critical under shear stress ($\phi_\tau \geq 1$). The circles represent results derived from the FE analyses and the upper and lower bounds are derived from Eqs. (16)–(17).

calculated from Eq. (17). The elastic critical buckling stress interaction curve is then deduced by substituting the relevant values into Eq. (16), allowing the determination of the elastic buckling stress of the full cross-section under the considered load case. Under direct stresses, plates are typically considered to be "long" since, in most cases, buckling stresses rapidly converge to the long plate solutions with increasing length; the long plate solutions are also lower bounds [1,4]. The same approach is taken in the present study. For very short plates, and

hence cross-sections, conservative results will be obtained; this will be explored further in future research.

6.3.1. Worked example: The elastic buckling stress of an I-section under combined shear and bending stress

Consider an I-section with geometric properties of $h_w = 1000$ mm, $t_w = 20$ mm, $a/h_w = 5$, $t_f/t_w = 1.5$, and $b_f/h_w = 0.2$, and material properties $E = 210$ kN/mm^2 and $\nu = 0.3$, subjected to combined shear and bending (i. e. $\psi = -1$).

The elastic buckling stress of the cross-section in shear is determined first by calculating the elastic buckling stresses of the isolated web and flange plates (using centreline geometry) using the expressions for the shear buckling coefficients k_τ shown in Table 2. For the flange, $a/b_f = 25$ and therefore

$$k^{\mathrm{SS}}_{\tau,\mathrm{f}} = 3.56 + 22/\left(a/b_f\right)^{3/2} = 3.56 + 22/(25^{3/2}) = 3.74, \tag{18}$$

$$k^{\mathrm{F}}_{\tau,\mathrm{f}} = 10 + 2.54/\left(a/b_f\right)^{3} = 10 + 2.54/(25^{3}) = 10.00, \tag{19}$$

and for the web,

$$k^{\mathrm{SS}}_{\tau,\mathrm{w}} = 5.34 + 4\left(h_w/a\right)^2 = 5.34 + 4/(5^2) = 5.50, \tag{20}$$

$$k^{\mathrm{F}}_{\tau,\mathrm{w}} = 8.98 + 5.60\left(h_w/a\right)^2 - 1.99\left(h_w/a\right)^3 = 8.98 + 5.60/(5)^2 - 1.99/(5)^3 = 9.19. \tag{21}$$

Hence,

$$\tau^{\mathrm{SS}}_{\mathrm{cr,f}} = 3.74\frac{\pi^2 \times 210 \times 10^3}{12\left(1-0.3^2\right)}\left(\frac{30}{200}\right)^2 = 15,954.60 \text{ N/mm}^2, \tag{22}$$

$$\tau^{\mathrm{F}}_{\mathrm{cr,f}} = 10.00\frac{\pi^2 \times 210 \times 10^3}{12\left(1-0.3^2\right)}\left(\frac{30}{200}\right)^2 = 42,705.71 \text{ N/mm}^2, \tag{23}$$

$$\tau^{\mathrm{SS}}_{\mathrm{cr,w}} = 5.50\frac{\pi^2 \times 210 \times 10^3}{12\left(1-0.3^2\right)}\left(\frac{20}{1030}\right)^2 = 393.59 \text{ N/mm}^2, \tag{24}$$

$$\tau^{\mathrm{F}}_{\mathrm{cr,w}} = 9.19\frac{\pi^2 \times 210 \times 10^3}{12\left(1-0.3^2\right)}\left(\frac{20}{1030}\right)^2 = 657.52 \text{ N/mm}^2, \tag{25}$$

from which $\tau^{\mathrm{SS}}_{\mathrm{cr,p}} = 393.59$ N/mm^2 and $\tau^{\mathrm{F}}_{\mathrm{cr,p}} = 657.52$ N/mm^2 are established.

Since $t_f/t_w = 1.5$, the maximum shear stress applied in the flange is

$$\tau_{\mathrm{max,f}} = \frac{1}{2}\frac{\tau_{\mathrm{max,w}} t_w}{t_f} = \frac{\tau_{\mathrm{max,w}}}{3}. \tag{26}$$

Substituting Eq. (26) into Eqs. (5)–(6), $\beta_{\tau,\mathrm{f}} = 3$ and $\beta_{\tau,\mathrm{w}} = 1$, which together with $\tau^{\mathrm{SS}}_{\mathrm{cr,f}}$ and $\tau^{\mathrm{SS}}_{\mathrm{cr,w}}$ are substituted into Eq. (11) to determine ϕ_τ,

$$\phi_\tau = \frac{\beta_{\tau,\mathrm{f}}\tau^{\mathrm{SS}}_{\mathrm{cr,f}}}{\beta_{\tau,\mathrm{w}}\tau^{\mathrm{SS}}_{\mathrm{cr,w}}} = \frac{3 \times 15954.60}{393.59} = 121.608 \qquad \left(\phi_\tau \geq 1 \therefore \text{web-critical}\right). \tag{27}$$

From Table 4,

$$\zeta_\tau = 1 - \left(\frac{0.8}{\sqrt{\phi_\tau}}\frac{t_f h_w}{t_w b_f}\right) = 1 - \left(\frac{0.8}{\sqrt{121.608}} \times \frac{1.5}{0.2}\right) = 0.456, \tag{28}$$

and therefore

$$\tau_{\mathrm{cr,cs}} = \tau^{\mathrm{SS}}_{\mathrm{cr,p}} + \zeta_\tau\left(\tau^{\mathrm{F}}_{\mathrm{cr,p}} - \tau^{\mathrm{SS}}_{\mathrm{cr,p}}\right) = 393.59 + 0.456\,(657.52 - 393.59) = 513.92 \text{ N/mm}^2. \tag{29}$$

The elastic buckling stress of the full cross-section under pure-bending stress follows the methodology established in [4], where under pure major-axis bending $\beta_{\sigma,\mathrm{w}} = \beta_{\sigma,\mathrm{f}} = 1$ and,

$$k^{\mathrm{SS}}_{\sigma,\mathrm{f}} = 0.43, \qquad \sigma^{\mathrm{SS}}_{\mathrm{cr,f}} = 1836.32 \text{ N/mm}^2, \tag{30}$$

$$k^{\mathrm{F}}_{\sigma,\mathrm{f}} = 1.25, \qquad \sigma^{\mathrm{F}}_{\mathrm{cr,f}} = 5338.13 \text{ N/mm}^2, \tag{31}$$

$$k^{\mathrm{SS}}_{\sigma,\mathrm{w}} = 23.9, \qquad \sigma^{\mathrm{SS}}_{\mathrm{cr,w}} = 1710.33 \text{ N/mm}^2, \tag{32}$$

$$k^{\mathrm{F}}_{\sigma,\mathrm{w}} = 39.6, \qquad \sigma^{\mathrm{F}}_{\mathrm{cr,w}} = 2833.85 \text{ N/mm}^2. \tag{33}$$

Thus,

$$\phi_\sigma = \frac{\beta_{\sigma,\mathrm{f}}\sigma^{\mathrm{SS}}_{\mathrm{cr,f}}}{\beta_{\sigma,\mathrm{w}}\sigma^{\mathrm{SS}}_{\mathrm{cr,w}}} = 1.074, \tag{34}$$

and $\sigma^{\mathrm{SS}}_{\mathrm{cr,p}} = 1710.33$ N/mm^2 and $\sigma^{\mathrm{F}}_{\mathrm{cr,p}} = 2833.85$ N/mm^2. From Table 4,

$$\zeta_\sigma = \frac{t_f}{t_w}\left(0.45 - \frac{0.3}{\phi^2_\sigma}\right) = 1.5\left(0.45 - \frac{0.3}{1.074^2}\right) = 0.285, \tag{35}$$

hence,

$$\sigma_{\mathrm{cr,cs}} = \sigma^{\mathrm{SS}}_{\mathrm{cr,p}} + \zeta_\sigma\left(\sigma^{\mathrm{F}}_{\mathrm{cr,p}} - \sigma^{\mathrm{SS}}_{\mathrm{cr,p}}\right) = 1710.33 + 0.285\,(2833.85 - 1710.33) = 2030.12 \text{ N/mm}^2. \tag{36}$$

For pure major-axis bending, $\psi = -1$ which is substituted into Eq. (17) resulting in $p = 2$. The solutions are substituted into Eq. (16) to derive the relationship for the elastic buckling stress of the cross-section under combined shear and bending, given by:

$$\left(\frac{\sigma}{\sigma_{\mathrm{cr,cs}}}\right)^2 + \left(\frac{\tau}{\tau_{\mathrm{cr,cs}}}\right)^2 = 1, \tag{37}$$

which is depicted by the blue line in Fig. 12 for this worked example.

6.3.2. Evaluation of full cross-section predictions

The performance of the methodology proposed is evaluated by superimposing the results from the FE analysis, shown as black circles in Fig. 12, noting that the results that lie beyond the blue prediction curve represent safe estimates. To evaluate the performance of the prediction, the length of the line between the origin and the FE result $\left(L_{\mathrm{FE}}\right)$ is determined, together with the length of the same line and its intersection with the prediction curve $\left(L_{\mathrm{pred}}\right)$, as shown in Fig. 12. The prediction ratio (R_{pred}) is evaluated using the expression:

$$R_{\mathrm{pred}} = \frac{L_{\mathrm{pred}}}{L_{\mathrm{FE}}}. \tag{38}$$

The same procedure is adopted to calculate the prediction ratio for the response if the panels are considered in isolation $\left(R_{\mathrm{EC3}}\right)$ using the expression,

$$R_{\mathrm{EC3}} = \frac{L_{\mathrm{isol}}}{L_{\mathrm{FE}}}, \tag{39}$$

where L_{isol} is the length from the origin and the simply-supported prediction.

A total of 527 I-sections, with different t_f/t_w, b_f/h_w and a/h_w combinations as described previously, were each subjected to the 11 combined load cases, described by Eq. (15), for each (τ, ψ) load combination. Thus, for each (τ, ψ) combination, 5797 data points resulted from the parametric study. The prediction ratios defined in Eqs. (38)–(39) are calculated for all the data points, and evaluated using normalised frequency distribution plots shown in Fig. 13. The mean predicted full cross-section local buckling stress is typically within 7% of the numerical results while the CoV is in the range 0.05–0.09, indicating the very low degree of scatter within the predictions. Hence, the proposed functions are again shown to be accurate and consistent, with clear benefits over the traditional approach of ignoring plate element interaction.

7. Conclusions

This paper presents formulae for calculating the elastic local buckling stresses of doubly-symmetric thin-walled I-sections subjected to shear stresses alone and in combination with direct stresses. The elastic buckling stresses of doubly-symmetric I-sections with a wide range of geometric properties were determined using finite element (FE) models,

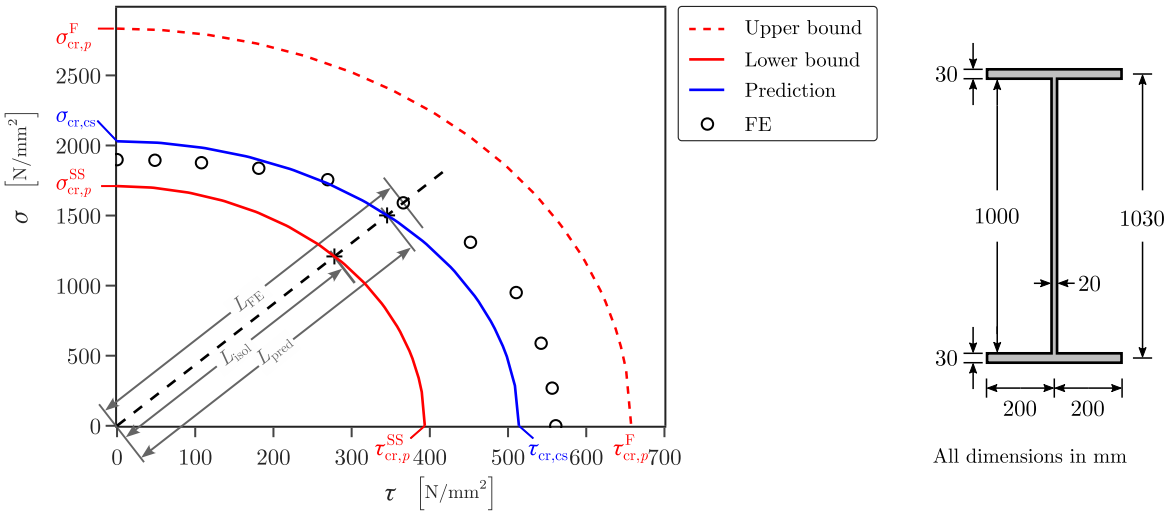


Fig. 12. Determining the buckling coefficient for cross-section with $h_w = 1000$ mm, $t_w = 20$ mm, $a/h_w = 5$, $t_f/t_w = 1.5$, and $b_f/h_w = 0.2$, subjected to combined shear and bending stresses. (For interpretation of the references to colour in this figure legend, the reader is referred to the web version of this article.)

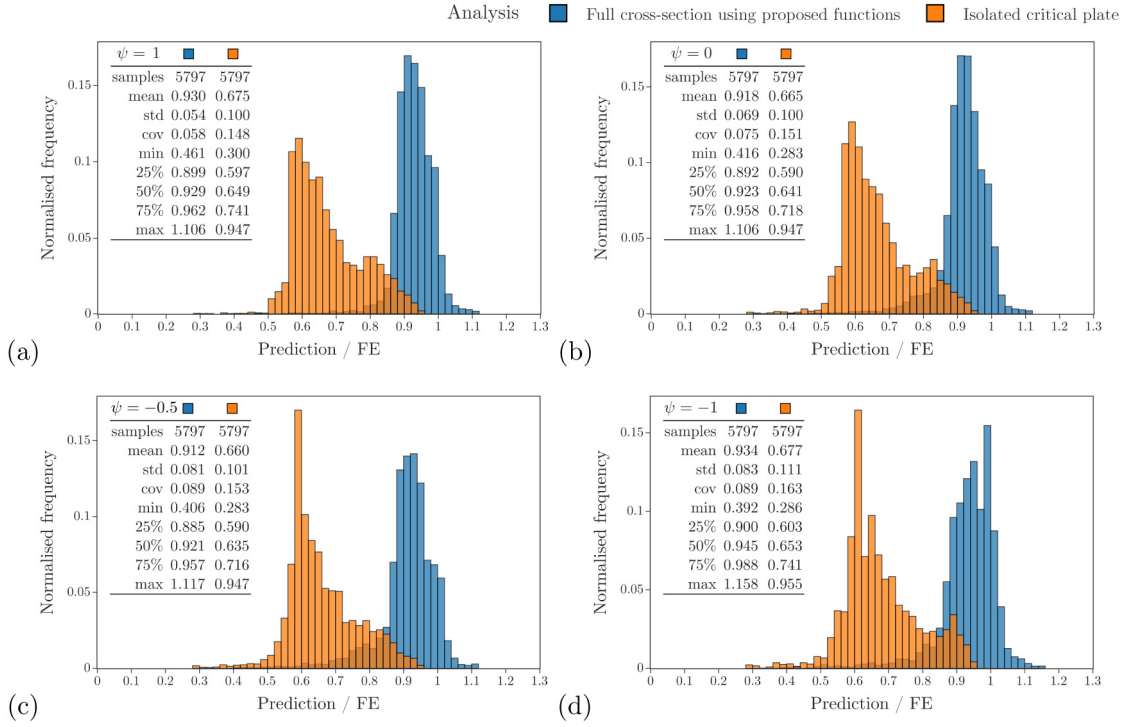


Fig. 13. Normalised frequency distribution for buckling stress predictions of full cross-sections subjected to shear stress and direct stress with ψ values of (a) 1 (compression), (b) 0, (c) −0.5, (d) −1 (bending).

the results of which correlate well with previous results derived in [4] using the finite strip method, and published results from analytical studies. The local buckling stress of the entire cross-section is shown to lie between the elastic buckling stress of the critical isolated plate within the cross-section with simply-supported and fixed boundary conditions along the adjoined edges. While the upper and lower bound limits for the internal plate element (web) were clearly defined in the literature, the buckling of outstand flange plates under shear had not been widely studied previously, and thus were examined in the present paper. Simplified expressions to predict the shear buckling coefficient of outstand plates are presented and shown to provide accurate predictions of the FE results.

The effect of element interaction on the overall elastic buckling stress of I-sections is accounted for via an interaction coefficient ζ_τ. The results of the FE models were used to calibrate simple closed form expressions to predict this interaction coefficient. The proposed concept was extended to consider the elastic buckling stress of the I-section under combined direct and shear stresses. Using the developed formulae, the elastic local buckling stresses of the studied cross-sections are accurately predicted, typically within 5% of the values obtained from FE models; this is a significant improvement over the results determined in the traditional manner where plate element interaction effects are ignored, where the full cross-section buckling stress is shown to be underestimated by as much as 40%. This improved elastic buckling stress prediction will have implications on the calculation of the ultimate shear strength of I-sections, which is currently being studied by the authors considering the cases of both flat and warped webs [27].

CRediT authorship contribution statement

Luke Lapira: Writing – original draft, Visualization, Validation, Methodology, Investigation, Formal analysis, Data curation, Conceptualization. **Leroy Gardner:** Writing – review & editing, Supervision, Investigation, Conceptualization. **M. Ahmer Wadee:** Writing – review & editing, Supervision, Investigation, Conceptualization.

Declaration of competing interest

The authors declare the following financial interests/personal relationships which may be considered as potential competing interests: Luke Lapira acknowledges the financial support provided by the President's Scholarship scheme from Imperial College London. Both Leroy Gardner and M. Ahmer Wadee serve on the Editorial Board for the journal "Thin-Walled Structures".

Data availability

Data will be made available on request.

Acknowledgement

Financial support for Luke Lapira was provided by the President's PhD Scholarship scheme from Imperial College London.

References

[1] EN1993-1-5, Eurocode 3 - design of steel structures – Part 1-5: Plated structural elements, 2006.
[2] C.H. Pham, G.J. Hancock, Shear buckling of thin-walled channel sections, J. Construct. Steel Res. 65 (3) (2009) 578–585, http://dx.doi.org/10.1016/J.JCSR.2008.05.015.
[3] M. Seif, B.W. Schafer, Local buckling of structural steel shapes, J. Construct. Steel Res. 66 (2010) 1232–1247, http://dx.doi.org/10.1016/J.JCSR.2010.03.015.
[4] L. Gardner, A. Fieber, L. Macorini, Formulae for calculating elastic local buckling stresses of full structural cross-sections, Structures 17 (2019) 2–20, http://dx.doi.org/10.1016/J.ISTRUC.2019.01.012.
[5] E. Stowell, E. Lundquist, Local Instability of Columns with I-, Z-, Channel, and Rectangular-Tube Sections, NACA Tech. Note 743, 1939.
[6] E. Lundquist, E. Stowell, Critical Compressive Stress for Flat Rectangular Plates Supported Along All Edges and Elastically Restrained Against Rotation Along the Unloaded Edges, NACA Special Report 189, 1941.
[7] E. Lundquist, E. Stowell, Critical compressive stress for outstanding flanges, NACA Report 734, 1942.
[8] S.C. Lee, J.S. Davidson, C.H. Yoo, Shear buckling coefficients of plate girder web panels, Comput. Struct. 59 (5) (1996) 789–795, http://dx.doi.org/10.1016/0045-7949(95)00325-8.
[9] B.W. Schafer, Review: The Direct Strength Method of cold-formed steel member design, J. Construct. Steel Res. 64 (7–8) (2008) 766–778, http://dx.doi.org/10.1016/J.JCSR.2008.01.022.
[10] C. Marsh, Influence of bend radii on local buckling in cold formed shapes, J. Struct. Eng. 123 (1997) 1686–1689, http://dx.doi.org/10.1061/(ASCE)0733-9445(1997)123:12(1686).
[11] V. Zeinoddini, B.W. Schafer, Impact of corner radius on cold-formed steel member strength, in: Twentieth International Specialty Conference on Cold-Formed Steel Structures, Vol. 1, 2010, pp. 1–15.
[12] L. Vieira, R. Gonçalves, D. Camotim, On the influence of the rounded corners on the local stability of RHS members under axial force and biaxial bending, Thin-Walled Struct. 144 (2019) 106327, http://dx.doi.org/10.1016/J.TWS.2019.106327.
[13] A. Fieber, L. Gardner, L. Macorini, Formulae for determining elastic local buckling half-wavelengths of structural steel cross-sections, J. Construct. Steel Res. 159 (2019) 493–506, http://dx.doi.org/10.1016/J.JCSR.2019.04.037.
[14] Dassault Systèmes Simulia Corp, ABAQUS/Standard, Version 2019, Providence, USA, 2019.
[15] R.V. Southwell, S.W. Skan, On the stability under shearing forces of a flat elastic strip, Proc. R. Soc. Lond. Ser. A Math. Phys. Eng. Sci. 105 (1924) 582–607, http://dx.doi.org/10.1098/rspa.1924.0040.
[16] M. Stein, J. Neff, Buckling Stresses of Simply Supported Rectangular Flat Plates in Shear, NACA Tech. Note 1222, 1947.
[17] S.P. Timoshenko, S. Woinowsky-Krieger, Theory of Plates and Shells, second ed., McGraw-Hill, New York, 1959.
[18] I.T. Cook, K.C. Rockey, Shear buckling of clamped and simply-supported infinitely long plates reinforced by closed-section transverse stiffeners, Aeronaut. Q. 13 (1962) 212–222, http://dx.doi.org/10.1017/s0001925900002432.
[19] P.S. Bulson, The Stability of Flat Plates, Chatto & Windus, London, 1970, http://dx.doi.org/10.1016/0016-0032(72)90156-1.
[20] S. Iguchi, Die knickung der rechteckigen platte durch schubkräfte, Ing.-Arch. 9 (1938) 1–12, http://dx.doi.org/10.1007/BF02084324.
[21] G.J. Hancock, C.H. Pham, Shear buckling of channel sections with simply supported ends using the semi-analytical finite strip method, Thin-Walled Struct. 71 (2013) 72–80, http://dx.doi.org/10.1016/J.TWS.2013.05.004.
[22] N. Saliba, E. Real, L. Gardner, Shear design recommendations for stainless steel plate girders, Eng. Struct. 59 (2014) 220–228, http://dx.doi.org/10.1016/j.engstruct.2013.10.016.
[23] X. Yun, L. Gardner, N. Boissonnade, Ultimate capacity of I-sections under combined loading – Part 2: Parametric studies and CSM design, J. Construct. Steel Res. 148 (2018) 265–274, http://dx.doi.org/10.1016/J.JCSR.2018.05.024.
[24] X. Meng, L. Gardner, A.J. Sadowski, J.M. Rotter, Elasto-plastic behaviour and design of semi-compact circular hollow sections, Thin-Walled Struct. 148 (2020) 106486, http://dx.doi.org/10.1016/J.TWS.2019.106486.
[25] E.Z. Stowell, E.B. Schwartz, Critical Stress for an Infinitely Long Flate Plate with Elastically Restrained Edges under Combined Shear and Direct Stress, NACA War Time Report WR-L-340, 1943.
[26] S. Way, Stability of rectangular plates under shear and bending forces, J. Appl. Mech. 3 (1936) A131–A135, http://dx.doi.org/10.1115/1.4008720.
[27] L. Lapira, M.A. Wadee, L. Gardner, Nonlinear analytical modelling of flat and hyperbolic paraboloidal panels under shear, Proc. R. Soc. Lond. Ser. A Math. Phys. Eng. Sci. 477 (2021) http://dx.doi.org/10.1098/RSPA.2021.0317.